Applied Catalysis B: Environmental 252 (2019) 128–137

Contents lists available at ScienceDirect

Applied Catalysis B: Environmental

journal homepage: www.elsevier.com/locate/apcatb

Metal-free carbon nitride photocatalysis with *in situ* hydrogen peroxide generation for the degradation of aromatic compounds

André Torres-Pinto, Maria J. Sampaio, Cláudia G. Silva, Joaquim L. Faria, Adrián M.T. Silva*

Laboratory of Separation and Reaction Engineering – Laboratory of Catalysis and Materials (LSRE-LCM), Faculdade de Engenharia, Universidade do Porto, Rua Dr. Roberto Frias, 4200-465 Porto, Portugal

ARTICLE INFO

Keywords:
Water treatment
Advanced oxidation processes
g-C_3N_4
Phenolic compounds
Hydrogen peroxide

ABSTRACT

The photocatalytic performance of a thermally exfoliated carbon nitride material was investigated in aqueous solution and employing visible-light emitting diodes (LEDs) as radiation source (λ_{max} = 417 nm). The operating conditions were studied using phenol as model compound. The increase on the surface area of the catalyst with the exfoliation treatment promotes faster degradation and mineralization rates and an easier reduction of O_2 into H_2O_2. The H_2O_2 production takes place only in the presence of both phenol and dissolved oxygen. The study was followed by assessing the photocatalytic degradation of ten organic compounds (individually or in a mixture) commonly found in agro-industrial wastewaters (phenol, catechol, resorcinol, hydroquinone, benzoic acid, 4-hydroxybenzoic acid, protocatechuic acid, gallic acid, 4-methoxyphenol and tyrosol). These compounds were selected to study the position, order and nature of substitution on the aromatic ring as well as the possible influence of the pK_a. Generally, more reactive compounds yield higher amounts of H_2O_2 formed, whereas the pK_a does not affect photocatalysis owing to the amphoteric properties of the catalyst. Thus, the successful oxidation of the organic compounds achieved in situ generation of H_2O_2 with relatively high productivities using a metal-free carbon nitride material stable in consecutive runs.

1. Introduction

The development of efficient and inexpensive technologies for wastewater treatment is important in the field of environmental protection. Aromatic compounds are present in many industrial and agro-industrial wastewaters, such as those from olive mills containing a high amount of organic matter and phenolic molecules. The development of an efficient and environmentally-safe treatment process remains a demanding issue.

Several reports have been published in the field of advanced oxidation processes (AOPs), particularly in visible light-driven photocatalysis, for the degradation of these pollutants [1–4]. Sunlight is a free and limitless supply of energy whose radiation works as driving force for the activation of several photocatalysts. However, light emitting diodes (LEDs) are also attracting major attention in this field, due to its low cost and respective flexibility to design photocatalytic reactors with different configurations and controlled irradiation features.

Carbon nitride, composed by layered polymeric triazine or tri-*s*-triazine (heptazine) networks comparable to graphitic planes, here designated as gCN, has appeared as a promising photocatalyst due to its optical semiconductor properties, ease of preparation, high physicochemical stability and flexible possibilities of functionalization for metal-free applications [5]. This material has adequate band gap with favourable energy band positions for photocatalytic H_2 formation, CO_2 reduction, organosynthesis and degradation of contaminants such as organic micropollutants found in urban wastewater treatment plant effluents (e.g., carbamazepine, isoproturon, clopidogrel, diclofenac, atenolol, bezafibrate, tramadol, venlafaxine, fluoxetine) [5–8]. Its structural properties, morphology, adsorption capacity, structure at micro- and nano-levels, among others, are also important. For instance, some authors reported that the macro and mesoporosity of the catalysts have influence on the scattering of light, highly porous materials yielding more photo-activated electrons [9,10].

Nevertheless, the pristine gCN material, i.e. the as synthesized product, has a small surface area, commonly resulting in more limited photocatalytic activity. Thus, several strategies have been pursued to design efficient gCN based photocatalysts, such as soft templating, exfoliation, elemental doping or heterojunction formation [5]. Many reports are focused either on coupling or doping gCN with metals (i.e., higher costs and concerns regarding leaching, overoxidation, among others), or using dyes as model organic substrates [11–13].

In the field of the photocatalytic degradation of aromatic molecules by using metal-free gCN materials, it has been noted that the respective

* Corresponding author.
E-mail address: adrian@fe.up.pt (A.M.T. Silva).

https://doi.org/10.1016/j.apcatb.2019.03.040
Received 8 January 2019; Received in revised form 7 March 2019; Accepted 14 March 2019
Available online 23 March 2019

mechanism is substantially different from that of the traditional P25 photocatalyst, hydrogen peroxide (H_2O_2) and other oxy-species, such as reactive oxygen species (ROS), being simultaneously produced via oxygen reduction [1,3,4,14,15].

In gCN photocatalysis, H_2O_2 can be produced under mild conditions (neutral pH, ambient temperature) in the presence of oxygen and an adequate hole scavenger. Several recent studies, focused on the H_2O_2 production with gCN catalysts, have reported the use of aliphatic alcohols as sacrificial agents acting as hole scavengers (e.g., propan-2-ol, ethanol, methanol) [16–19]. The degradation of aromatic molecules (i.e., hole scavengers) with simultaneous H_2O_2 generation is of particular interest for the development of water and wastewater treatment since H_2O_2 is an environmentally friendly oxidizing agent that under certain conditions can generate the highly reactive hydroxyl radicals ($HO^{\bullet}$) [4,15]. For instance, Zhang et al. studied the degradation of phenol and detected simultaneous formation of ROS, with comparatively higher H_2O_2 generation on an exfoliated gCN catalyst than on the pristine material [20].

Some mechanisms (Eqs. (1)–(4)) have been proposed for the photoactivation of this catalyst and the formation of ROS and H_2O_2 [21,22]. In those studies, the authors suggested that the activation of the catalyst with light ($h\nu$) originates the electron/hole (e^-/h^+) pairs – Eq. (1). Electrons are consumed by dissolved oxygen, forming H_2O_2 by the two–electron reduction reaction – Eq. (2). Then, H_2O_2 can form $HO^{\bullet}$ Eq. (3), whereas superoxide radicals ($O_2^{\bullet -}$) are generated by one-electron reduction of oxygen – Eq. (4). The organic compounds can be degraded by the photogenerated holes or by the ROS. However, this mechanism is not yet completely understood.

$$\text{photocatalyst} + h\nu \rightarrow e^- + h^+ \quad (1)$$

$$O_2 + 2\,e^- + 2\,H^+ \rightarrow H_2O_2 \quad (2)$$

$$H_2O_2 + e^- \rightarrow HO- + HO^{\bullet} \quad (3)$$

$$O_2 + e^- \rightarrow O_2^{\bullet -} \quad (4)$$

The main objective of the present study is to better understand the mechanisms involved in the abatement and mineralization of different aromatic compounds, with the simultaneous production of H_2O_2 using visible-LEDs as light source and gCN as a metal-free catalyst. To the best of our knowledge, the abatement of aromatic pollutants containing different substituent groups and the simultaneous H_2O_2 evolution in this metal-free photocatalytic system are followed for the first time in the present study.

2. Materials and methods

2.1. Chemicals and materials

Dicyandiamide ($C_2H_4N_4$, 99%), phenol (C_6H_5OH, ≥ 99%), titanium (IV) oxysulphate (TiO_5S, ~15 wt.% in sulphuric acid), H_2O_2 (30 wt.% in water), acetic acid ($C_2H_4O_2$, ≥ 99.8%), tyrosol ($C_8H_{10}O_2$, 98%) and resorcinol ($C_6H_6O_2$, 99%) were obtained from Sigma-Aldrich. Sodium sulphite anhydrous (Na_2SO_3, 98.5%) was obtained from Acros Organics. Hydroquinone ($C_6H_6O_2$, ≥ 99.5%) was obtained from Merck Millipore. Methanol (CH_4O, 99.99%) and acetonitrile (C_2H_3N, 99.99%) were obtained from Fisher Chemical. Sodium hydroxide (NaOH, 98.5%) was obtained from JMGS. Hydrochloric acid (HCl, ≥ 37%), sulphuric acid (H_2SO_4, 95.0–97.0%), sodium chloride (NaCl, ≥ 99.5%), catechol ($C_6H_6O_2$, ≥ 98%), benzoic acid ($C_7H_6O_2$, ≥ 99.5%), 4-hydroxybenzoic acid ($C_7H_6O_3$, ≥99.0%), protocatechuic acid ($C_7H_6O_4$, ≥ 97.0%), gallic acid ($C_7H_6O_5$, ≥ 98.0%) and 4-methoxyphenol ($C_7H_8O_2$, ≥ 98.0%) were obtained from Honeywell Fluka. Ultrapure water was produced in a Direct-Q Millipore system (Merck Millipore, Billerica, MA, USA).

2.2. Preparation and characterization of the catalyst

The synthesis of bulk carbon nitride (hereafter referred as gCN) was performed by thermal decomposition of dicyandiamide, as reported elsewhere [23]. Briefly, dicyandiamide was placed in a semi-closed crucible in a muffle furnace under static air atmosphere at 550 °C. Afterwards, the material was powdered in a mortar, rinsed with ultrapure water, filtered and dried overnight at 120 °C. The resulting powder was spread in an open crucible, placed in a muffle furnace and the temperature was maintained at 500 °C for 2 h. The final material was labelled as gCN-T.

The morphology of the catalysts was studied by scanning electron microscopy (SEM) using a FEI Quanta 400FEG ESEM/EDAX Genesis X4 M instrument. As previously reported [23], the Brunauer-Emmett-Teller (BET) specific surface area (S_{BET}) of the photocatalysts were determined from N_2 adsorption-desorption isotherms at −196 °C obtained in a Quantachrome Nova 4200e apparatus. For the point of zero charge (PZC) measurements, six solutions of 50 mL of NaCl 0.01 M were prepared with pH ranging from 2 to 12, using solutions of 0.1 and 0.01 M HCl, and 0.1 and 0.01 M NaOH. After that, 150 mg of gCN-T was added to each solution and left for 24 h with continuous stirring in the dark. Finally, the pH value of the PZC was determined from the interception of the final pH *v.* initial pH line with the diagonal line of the graph.

2.3. Photocatalytic experiments

A glass reactor with a maximum capacity of 80 mL was employed in the photocatalytic experiments. The photocatalytic reactions were performed under visible light irradiation using 10 W LEDs with a maximum emission line peak at 417 nm, located symmetrically from the outside at 4.0 cm from the reactor wall. The average irradiance (reaching the reactor wall) for each LED was ca. 400–500 W m^{-2}, as determined by UV–vis spectroradiometry using an OceanOptics USB2000 + UV–vis spectrometer. To achieve the adsorption-desorption equilibrium, 50 mL of an aqueous suspension containing the pollutant and a certain amount of catalyst was stirred in the dark for 30 min, and continuously bubbled with an air flow. Under these conditions, the concentration of the studied pollutants never decreased more than 10.0%. The initial concentration of each pollutant was kept at 0.64 mmol L^{-1} (equivalent to 60 mg L^{-1} of phenol) and the catalyst load varied from 0.1 to 1.0 g L^{-1}. After centrifugation and filtration, the collected samples were analysed as described below. For studying the effect of the O_2 partial pressure (resulting in varying concentrations of oxygen dissolved in the liquid phase), different mixtures of O_2 and Ar were saturated in the suspensions, whose composition were controlled by using Bronkhorst High-Tech EF-FLOW Select F-201 CV thermal mass flow meters. Reutilization tests were also performed. In this case, before reuse, the catalyst was thoroughly washed with ultrapure water and then dried at 120 °C for 12 h.

2.4. Analytical techniques

Samples periodically withdrawn from the photocatalytic reactor were analysed by high performance liquid chromatography (HPLC) using a Hitachi Elite LaChrom instrument (Hitachi, Ibaraki, Japan) equipped with a diode array detector (L-2450), a Purospher Star RP-18 column (250 mm × 4.6 mm, 5 µm particles), and a solvent delivery pump (L-2130) at a fixed flow rate of 1 mL min^{-1}. Each compound was analysed at the maximum absorption wavelength (λ_{max}). In the case of phenol (λ_{max} = 270 nm), catechol (λ_{max} = 274 nm), resorcinol (λ_{max} = 272 nm) and hydroquinone (λ_{max} = 288 nm), the HPLC method starts with an equilibrated mixture of water (A):methanol (B) (70:30) followed by a linear gradient step to A:B (37:63) in 20 min. Finally, the initial conditions were re-established in a 1 min gradient step and the A:B (70:30) mixture was isocratically eluted for 7 min. For benzoic acid (λ_{max} = 270 nm), 4-

hydroxybenzoic acid (λ_{max} = 250 nm), protocatechuic acid (λ_{max} = 254 nm), gallic acid (λ_{max} = 264 nm), 4-methoxyphenol (λ_{max} = 286 nm) and tyrosol (λ_{max} = 274 nm), the concentration of the individual compounds was followed using an optimized gradient elution method at a flow rate of 1 mL min^{-1}. Firstly, the column was equilibrated with an A:B (10:90) mixture of 1% acetic acid and 0.5% acetonitrile in methanol (A) and 1% acetic acid in water (B). Then, the following program was used: isocratic elution for 15 min followed by a linear gradient run to A:B (60:40) in 27 min and finally to A:B (10:90) in 5 min. Additionally, the concentration of aliphatic acids originated from the degradation of phenol was analysed in a Hitachi Elite LaChrom instrument equipped with a UV detector and read at λ = 200 nm. The HPLC method consisted on an isocratic elution with 5 mM of H_2SO_4 and flow rate of 0.5 mL min^{-1} in a Grace Alltech OA1000 column (300 mm × 6.5 mm).

The colorimetric method was used for the determination of the amount of H_2O_2 produced during the photocatalytic reactions [24]. Briefly, 300 µL of the filtered sample, 300 µL of 0.5 M H_2SO_4 and 10 µL of titanium(IV) oxysulphate were mixed in a polystyrene cuvette and the absorbance read at a wavelength of 405 nm by using an OceanOptics USB2000 + UV–vis spectrometer.

The total organic carbon (TOC) content was determined using a Shimadzu TOC-5000 A apparatus. The samples were withdrawn from the reactor, centrifuged, filtered and mixed with an excess of sodium sulphite (± 2 mg) in order to decompose some remained H_2O_2. The pH was measured in a pH 211 Microprocessor pH meter (HANNA Instruments). Dissolved oxygen (DO) and temperature of the solutions were determined using a Crison Oxi 45 portable oximeter.

3. Results and discussion

3.1. Catalyst characterization and mechanistic insights

The morphology of gCN and gCN-T samples was analysed by SEM (Fig. 1). The bulk material (gCN) is composed by compact aggregates, whereas gCN-T consists of thin separated layers of carbon nitride due to the thermal exfoliation. The electrostatic interactions between the carbon nitride layers (van der Waals forces) are broken during the thermal exfoliation, occurring the splitting of these layers. As reported previously [23], the higher S_{BET} of gCN-T (87 $m^2 g^{-1}$), compared to gCN (4 $m^2 g^{-1}$), may promote the efficiency of the gCN-T catalyst.

The gCN-T material was previously characterized [23], with respect to its enhanced photocatalytic activity for the conversion of benzyl alcohol into benzaldehyde. In addition to that characterization, we describe now the results on the acid/base and electrostatics of the material's surface. The PZC of both materials was determined in order to characterize their surface chemistry and understand the influence of the pH solutions in contact with the photocatalysts. As well described in literature, the gCN structure presents primary, secondary and tertiary amine groups [5]. Primary and secondary amines can react with both HO^- and H^+ from the solution (amphoteric nature) while tertiary amine groups can only accept H^+ [25]. The Eqs. ((5)–(9)) show the changes in carbon nitride surface charges, based on the equilibrium between the amino groups from the melem units with the reactive medium [26].

$$\equiv C{-}NH_2 + H^+ \rightarrow \equiv C{-}NH_3^+ \quad (5)$$

$$\equiv C{-}NH_2 + HO^- \rightarrow \equiv C{-}NH^- + H_2O \quad (6)$$

$$(\equiv C)_2{-}NH + H^+ \rightarrow (\equiv C)_2{-}NH_2^+ \quad (7)$$

$$(\equiv C)_2{-}NH + HO^- \rightarrow (\equiv C)_2{-}N^- + H_2O \quad (8)$$

$$(\equiv C)_3{-}N + H^+ \rightarrow (\equiv C)_3{-}NH^+ \quad (9)$$

A pH_{PZC} value of 6.0 was found for gCN-T (Fig. 2), therefore the material surface is negatively charged for pH values greater than 6.0

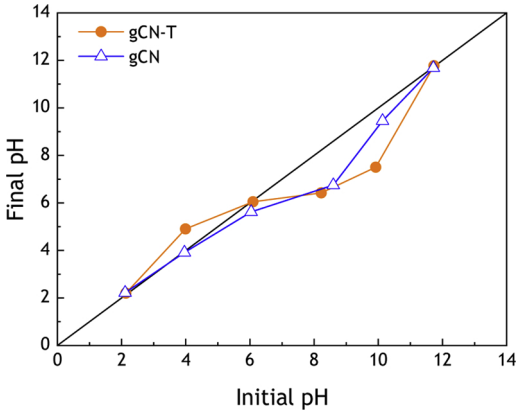

Fig. 2. PZC determination for gCN-T and gCN materials.

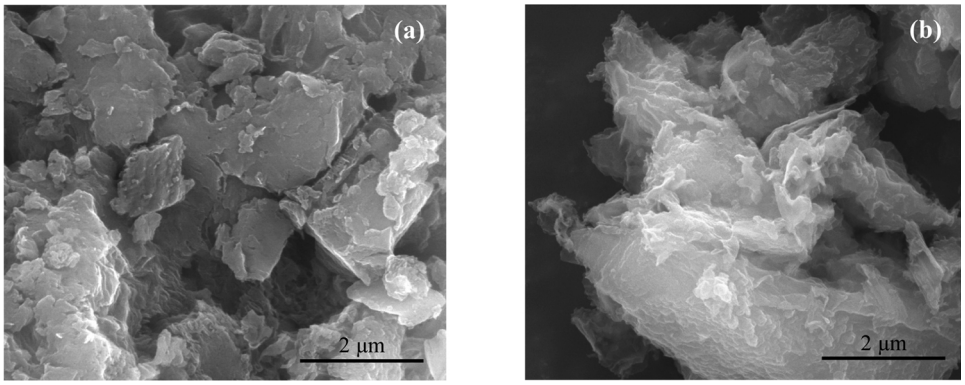

Fig. 1. SEM micrographs of **(a)** gCN and **(b)** gCN-T.

and positively charged for lower pH values. In contrast, the bulk material shows a pH_{PZC} of 3.4. Depending on the precursor used for the synthesis of gCN, different values of pH_{PZC} can be found in the literature: for cyanamide 4.1, thiourea 4.4, melamine 5.0 and urea 5.1 [26,27]. Thus, it seems that the use of distinct precursors and the preparation procedure have an important role on the physical-chemical properties of the surface of gCN materials.

The band gap energy of gCN-T, determined from the corresponding Tauc plot (Fig. SI1), is 2.73 eV, which is higher than the gCN material (2.68 eV). The valence (VB) and conduction (CB) band potentials were calculated for gCN-T using the Eqs. (10) and (11) [28]:

$$E_{VB} = X - E^{\circ} + 0.5\,E_g \quad (10)$$

$$E_{CB} = E_{VB} - E_g \quad (11)$$

where E_{VB} corresponds to the VB edge potential, E_{CB} to the CB edge potential, X is the electronegativity of a semiconductor obtained as a geometric mean of the constituent atoms (4.5 eV for gCN [29]), E° is energy of free electrons *v.* vacuum (4.5 eV) and E_g is the band gap potential (determined from the Tauc plots). With those values the potentials for E_{VB} and E_{CB} are 1.51 eV and −1.22 eV, respectively.

3.2. Photocatalytic removal of phenol

The photocatalytic reactions were firstly investigated using phenol as model aromatic compound. Results showed a negligible photochemical degradation of phenol under visible light (Fig. 3a) owing to the lack of absorption of phenol above 300 nm (the irradiation system consists on LEDs with maximum emitted at 417 nm, Fig. SI2).

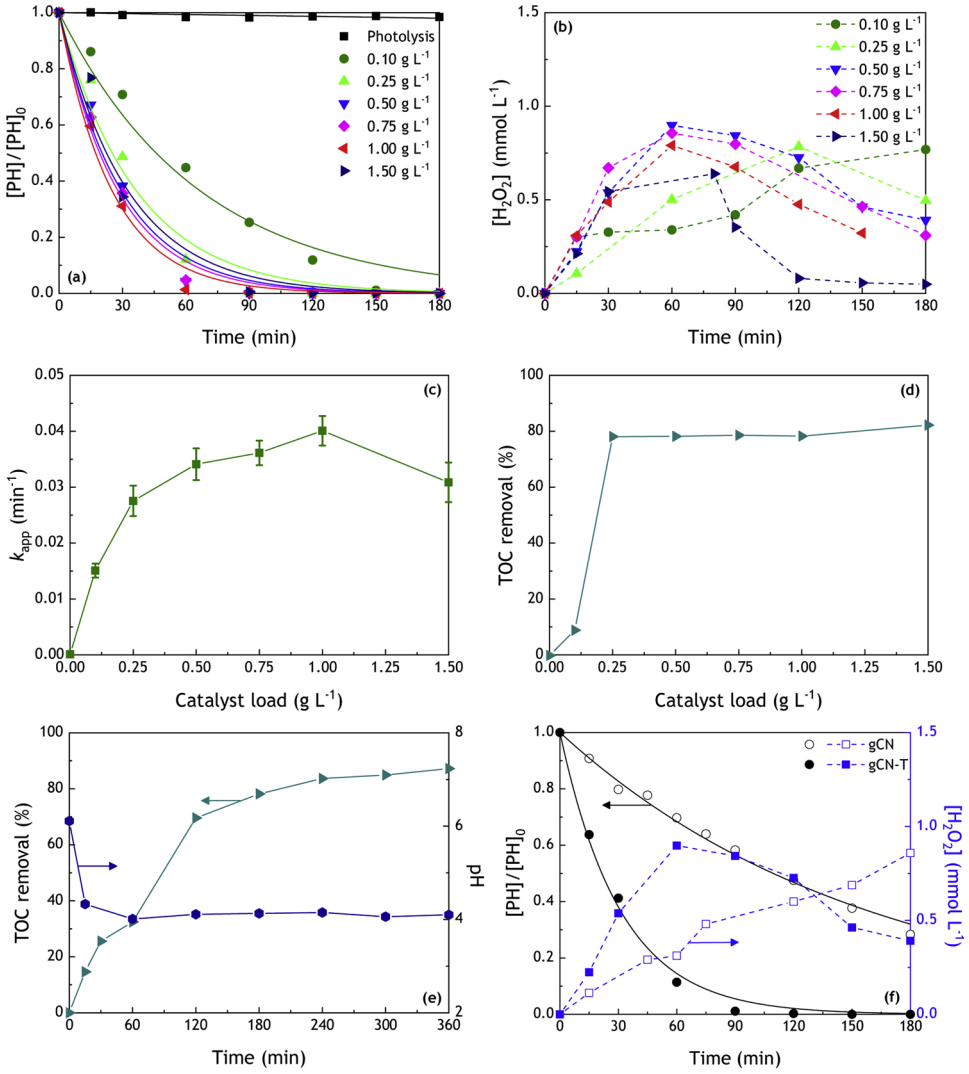

Fig. 3. (a) Phenol normalized concentration ($[PH]/[PH]_0$; $[PH]_0 = 60\,mg\,L^{-1}$) and **(b)** H_2O_2 production as a function of reaction time; **(c)** apparent first-order reaction rate constant (k_{app}) as a function of catalyst load; **(d)** TOC removal for different gCN-T catalyst loads after 180 min of reaction; **(e)** TOC removal and pH as a function of time for a 0.50 g L^{-1} gCN-T load; **(f)** $[PH]/[PH]_0$ and H_2O_2 production using gCN and gCN-T.

Moreover, H_2O_2 was not formed in the absence of any photocatalyst.

The reaction rate (r) in heterogeneous photocatalysis systems commonly follows an exponential decay, based on the Langmuir-Hinshelwood mechanism [30,31]. Under oxygen saturation conditions of the liquid phase, the normalized concentration of the pollutant (C/C_0) can be represented as a function of time (Fig. 3a) and the apparent first-order reaction rate constant (k_{app}) can be obtained by fitting an exponential decay model (Fig. 3c).

In order to avoid an excess of catalysts and to ensure an efficient absorption of photons reachingthe target molecule, the influence of the catalyst load in the efficiency of the process was studied. The photocatalyst load was varied between 0.10 and 1.50 g L^{-1}. A compromise between phenol degradation (Fig. 3a) and H_2O_2 formation (Fig. 3b) was found for 0.5 g L^{-1} of catalyst load. In this case, 90% of phenol removal and 0.90 mmol L^{-1} of H_2O_2 concentration are achieved after 60 min of reaction. A slight increase in k_{app} (Fig. 3c) was observed for a higher catalyst load of 1.00 g L^{-1} (0.040 min^{-1}) compared with 0.50 g L^{-1} (0.033 min^{-1}), however lower H_2O_2 formation was achieved (Fig. 3b). It is worth mentioning that the H_2O_2 concentration increases and then decreases with an exception for the lowest catalyst load (0.10 g L^{-1}), the maximum H_2O_2 concentration normally being reached when phenol is nearly completely degraded (Fig. 3a), i.e. at 60 min. The capacity of a semiconductor to drive H_2O_2 production from O_2 mostly depends on its electronic properties, since the band gap potential may enable one-electron or four-electron O_2 reduction, respectively leading to $O_2^{\bullet -}$ or water formation, and decreasing the selectivity towards H_2O_2 generation [17,32]. For instance, the adsorbed oxygen on the surface of a bulk gCN material is preferably reduced to $O_2^{\bullet -}$ via one–electron [20], while on modified gCN catalysts, with more surface defects, O_2 preferably suffers two-electron reduction to form H_2O_2. The reduction of dissolved O_2 to form H_2O_2 (Eq. (2)) and $O_2^{\bullet -}$ (Eq. (4)) show potentials of $E_0 = -0.33$ and $+0.281$ V *v.* SHE at pH = 7, respectively [33]. Moreover, dissolved O_2 can also be reduced to water by a four-electron reaction ($E_0 = +0.815$ V *v.* SHE at pH = 7 [33]). When H_2O_2 is formed, it can be then reduced to yield $HO^{\bullet}$ radicals (Eq. (3)) or oxidized to water ($E_0 = +0.38$ and $+1.349$ V *v.* SHE at pH = 7, respectively [33]). Since the CB energy level of gCN-T is -1.22 eV, and according to its redox potentials, the reduction reactions with the CB e^- are expected in the following order: Eq. (4) ≥ Eq. (3) > Eq. (2). On the VB, the direct oxidation of phenol with photoactivated h^+ occurs and has a potential of +1.76 V [28]. Therefore, the reactive species presumably responsible for the oxidative attack of the aromatic molecules are the photogenerated h^+ and the radicals obtained by reduction reactions on the CB.

In terms of mineralization, remarkable TOC removals are achieved in 180 min for catalyst loads higher than 0.25 g L^{-1} (Fig. 3d), reaching a plateau at an average 79.1% removal. As example, the TOC removals determined at different reaction times for 0.50 g L^{-1} are shown in Fig. 3e, values of 77.2 and 87.2% being measured after 180 and 360 min, respectively. Typical aromatic reaction intermediates occurring in phenol oxidative photodegradation (catechol, benzoquinone and hydroquinone [34]) were below the limit of analysis detection, whereas low molecular weight carboxylic acids were detected (formic, fumaric, maleic and malonic acids), but not quantified due to their very low concentrations. In agreement, at these experimental conditions, the initial pH of 6 decreased to 4 in 30 min (Fig. 3e). Moreover, a control experiment under similar conditions but performed in the dark showed that the TOC remains constant, making clear the need of light for the mineralization process to occur.

Finally, the performance of gCN and gCN-T materials was compared (Fig. 3f). Using 0.50 g L^{-1} of gCN, incomplete degradation of phenol was observed even after 180 min of reaction, whereas this organic compound is degraded with gCN-T to levels below the detection limit in less than 90 min, the k_{app} (0.034 min^{-1}) being five times higher than with gCN (k_{app} = 0.006 min^{-1}). The production of H_2O_2 was similarly decelerated with gCN, a maximum concentration of 0.86 mmol L^{-1} being achieved only after 180 min (at variance with the higher H_2O_2 concentration achieved for gCN-T in 60 min), as well as a lower TOC reduction (45.5%) was achieved. These differences are observed owing to the improved photoefficiency of the exfoliated material. Thus, the photocatalytic efficiency enhancement using gCN-T is mainly ascribed to its increased surface area, ensuing higher availability of active sites when compared to the initial gCN, since the band gap of these materials is similar. The surface area can play a major role on heterogeneous photocatalysis allowing for redox reactions to occur more easily due to stronger contact between adsorbed reactants and the surface-active sites [35]. In fact, several authors have shown that the surface area increase of carbon nitride based materials leads to higher efficiency of the photocatalytic process (faster pollutant degradation rates [3,36] and higher yields of H_2O_2 [14,15]).

3.3. H_2O_2 production with gCN-T

As described before, a maximum H_2O_2 concentration was obtained at 60 min of reaction when almost complete phenol degradation was achieved (Fig. 3b). After that time, the H_2O_2 concentration starts to decrease since phenol was completely removed from the solution. H_2O_2 is expected to be produced in the presence of gCN-T, of a proton donor (such as phenol) and molecular oxygen. To better understand this mechanism, the H_2O_2 formation and decomposition phenomena were studied separately by changing selected reaction conditions.

To study the H_2O_2 formation, a specific set of experiments were performed, by selectively removing: (i) the molecular oxygen; (ii) the proton donor, i.e. phenol; (iii) the photocatalyst; or (iv) the light. No H_2O_2 formation was found for any of these reactions, indicating that the presence of all the components is a *sine qua non* condition.

To investigate the H_2O_2 decomposition, another set of experiments were performed, in this case adding H_2O_2 at the beginning of each run (c.a. 1–3 mmol L^{-1}) under the same above described (i) to (iv) experimental conditions. Results showed that no decomposition of H_2O_2 takes place in the absence of photocatalyst and light source. Moreover, the concentrations of both phenol and H_2O_2 remained the same under dark conditions, demonstrating that phenol is not removed by adsorption on the catalyst surface.

In another experiment, performed in the presence of all components (H_2O_2, oxygen, phenol, gCN-T and light), H_2O_2 is formed until nearly all phenol was degraded (60 min), then being decomposed. However, in the absence of phenol, with or without oxygen, H_2O_2 was fully decomposed proving that the pollutant and oxygen are not responsible for the decomposition of H_2O_2. Thus, the H_2O_2 decomposition occurs in the presence of the photoactivated gCN-T catalyst through reduction with the photogenerated electrons in the CB. Moreover, the phenol conversion is enhanced with argon saturation and in the presence of H_2O_2, in comparison to argon alone (Fig. SI5). Most probably, H_2O_2 is decomposed, producing radical species, such as $HO^{\bullet}$ radicals.

Finally, it is interesting to refer that a significantly higher k_{app} for phenol removal was obtained in the presence of oxygen (k_{app} = 0.044 min^{-1}) when compared to an experiment in the absence of oxygen (k_{app} = 0.004 min^{-1}).

Thus, these results indicate that the formation of H_2O_2 is due to the presence of dissolved oxygen and a proton donor reacting via the photoactivated catalyst, and that H_2O_2 suffers photocatalysis in anoxic conditions.

3.4. Influence of dissolved oxygen

The influence of dissolved O_2 on both phenol degradation and H_2O_2 production was also studied in detail. Several experiments were performed varying the ratio of oxygen to argon (O_2:Ar) in the gas feed (Fig. 4). In general, the dissolved oxygen (DO) content (not shown) initially decreases and then reaches a plateau when phenol is completely removed, i.e. at 120, 90 and 60 min for the 10, 21 and 100% O_2 feeds, respectively. Moreover, a faster phenol degradation is observed in the more O_2-rich solutions (Fig. SI3), e.g., k_{app} = 0.063 min^{-1} for 100% O_2, compared with the k_{app} = 0.001 min^{-1} under deoxygenated conditions (0% of O_2), as shown in Fig. 4. Under deoxygenated conditions, H_2O_2 production was not detected. On the other hand, increasing

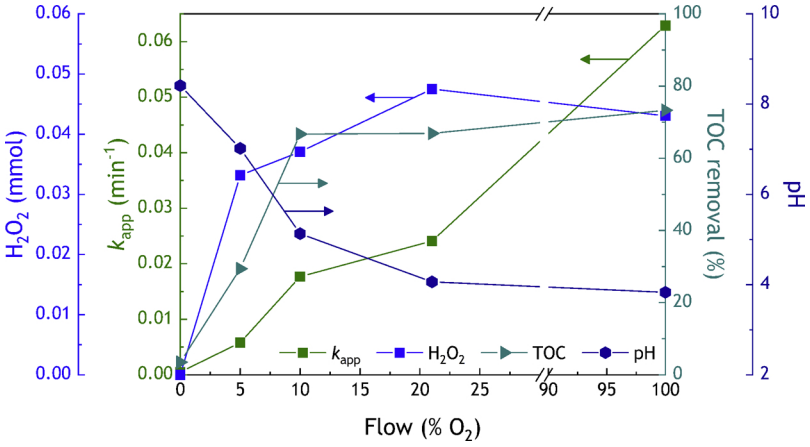

Fig. 4. Apparent first-order reaction constants (k_{app} –■–), highest amount of H_2O_2 generated (–■–), TOC removal (–▸–) and pH value (–●–) at 180 min for the photocatalytic degradation of phenol with different percentages of O_2:Ar feeds (constant gas flow, constant pressure: 2 bar).

the O_2 percentage (Fig. SI4), the highest H_2O_2 concentrations (0.66, 0.74, 0.95 and 0.86 mmol L^{-1} for 5, 10, 21 and 100% of O_2, respectively) were reached at 180, 150, 120 and 60 min, respectively. Thus, in general, higher DO contents lead to the highest H_2O_2 concentrations in shorter irradiation times.

The pH and TOC content were also determined in these experiments at the end of the photocatalytic reaction. Results showed that the TOC removal, k_{app} and amount of H_2O_2 generally increases with the percentage of O_2 in the solution, whereas the pH decreases (Fig. 4). However, for 21% and 100% of O_2, the amounts of H_2O_2 produced are quite similar. The excess oxygen may be reacting with photoactivated electrons, forming $O_2^{\bullet -}$ radicals, which may accelerate the degradation process and can explain the similar H_2O_2 evolved amounts. These radicals, together with $HO^{\bullet}$ and h^+ (detected indirectly from a scavenger reaction, Fig. SI5a), are the oxidizing species responsible for the pollutant degradation and mineralization.

Another important aspect to be taken into consideration is the general correlation existing between the four evaluated parameters (Fig. 4). Higher percentages of oxygen in the injected gas flow reveal a tendency to increase the phenol degradation (i.e., higher k_{app}), as well as the mineralization rate up to 10% O_2, whereas a lower pH is obtained at the end of the reaction. These results explain the oxidative attack by the generated radicals, promoting the photocatalytic degradation and mineralization of phenol, yielding an acidic final solution. In sum, more O_2 leads to a faster phenol removal and higher H_2O_2 production rates up to a certain value (ca. 0.04 mmol).

3.5. Degradation of different aromatic compounds

Ten aromatic compounds were chosen to study the photocatalytic

Table 1
Selected aromatic compounds and respective results after individual photocatalysis (highest amount of H_2O_2 produced, apparent first-order rate constant (k_{app}) and TOC removal).

Compound	Chemical structure	k_{app} (min^{-1})	TOC removal (%)	Maximum H_2O_2 evolved (mmol)[a]	H_2O_2 production rate (μmol g_{cat}^{-1} h^{-1})[a,b]
Phenol (PH)		0.034 ± 0.002	76.3	0.045 (60 min)	2151 (30 min)
Catechol (CT)		0.034 ± 0.003	77.8	0.031 (75 min)	1181 (30 min)
Resorcinol (RC)	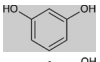	0.062 ± 0.006	76.8	0.052 (60 min)	3103 (15 min)
Hydroquinone (HQ)	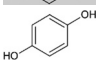	0.0059 ± 0.0001	69.3	0.021 (180 min)	633 (75 min)
Benzoic acid (BA)		0.0065 ± 0.0001	46.0	0.018 (120 min)	625 (30 min)
4-Hydroxybenzoic acid (HBA)	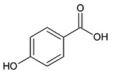	0.026 ± 0.002	77.7	0.045 (90 min)	2030 (15 min)
Protocatechuic acid (PCA)	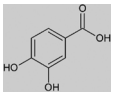	0.021 ± 0.003	72.9	0.044 (90 min)	2479 (15 min)
Gallic acid (GA)	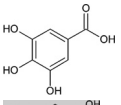	0.028 ± 0.003	70.9	0.047 (90 min)	1779 (15 min)
4-Methoxyphenol (MOP)	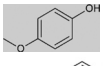	0.043 ± 0.003	52.1	0.042 (90 min)	1776 (15 min)
Tyrosol (TYR)	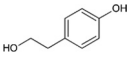	0.065 ± 0.004	43.4	0.035 (120 min)	2049 (15 min)

[a] The times in brackets correspond to when the values were obtained or calculated.
[b] Calculation based on highest measured H_2O_2 concentration at a given time. H_2O_2 production rate = H_2O_2 concentration (μmol L^{-1}) ÷ [catalyst load (g_{cat} L^{-1}) × irradiation time (h)].

degradation mechanism using gCN-T. These compounds are commonly found in olive mill wastewaters [37–39] and were selected according to their chemical structure in order to study the impact of the position, order and nature of substitution on the aromatic ring, comparatively to phenol. No significant degradation was observed by photolysis, and no H_2O_2 was produced (results not shown). These results were expected considering that the emission spectrum of the LEDs (Fig. SI2) and the absorption spectra of the compounds tested do not match. The photocatalytic results are summarized in Table 1: k_{app}, TOC removal, maximum amount of H_2O_2 and respective production rate.

Catechol (CT), resorcinol (RC) and hydroquinone (HQ) were selected for this study as they have two −OH groups in the *ortho*, *meta* and *para* positions (comparing to phenol - PH), respectively. As expected a faster degradation was observed for RC, then PH, CT and HQ (Fig. 5a, Table 1, a zero-order reaction model being more likely in the specific case of HQ). This is due to the activating nature of the −OH group which is *ortho* and *para* director for electrophilic substitution [40]. In this sense, a hole generated in gCN-T will act as the electrophile and the degradation process will be initiated by the attack on the aromatic ring. The RC ring can be easily attacked in three distinct carbon atoms; phenol as well but in a lesser extent. Then, CT and HQ are more difficult to be decomposed since all carbon atoms are less prone to be attacked owing to the position of the −OH substituents [40]. PH and RC yield the highest amounts of H_2O_2 (Fig. 5b), as they are the most reactive, achieving the maximum H_2O_2 concentration at 60 min (corresponding to 0.045 and 0.052 mmol of H_2O_2, respectively). H_2O_2 production reaches a maximum at 75 min (0.031 mmol) during the degradation of CT, whereas 0.021 mmol of H_2O_2 are obtained for HQ at 180 min.

Benzoic acid (BA), 4-hydroxybenzoic acid (HBA), protocatechuic acid (PCA) and gallic acid (GA), with none, one, two and three −OH groups, respectively, were selected to study the influence of the number of strong electron-donating −OH groups on the ring over the common strong electron-withdrawing −COOH group. The differences were less notorious in this case, but the degradation was faster for GA and HBA, then PCA and lastly BA (Fig. 5c). The influence of the −OH group is more predominant relatively to the −COOH group due to their relative strengths [40]. In addition, the presence of more −OH groups can further protect or activate the ring according to their positions. GA has three very strong activating groups (−OH) and a strongly deactivating group (−COOH), thus the combination of these substituents makes GA to be easily degraded. BA has only one electron-withdrawing group, being the less reactive of these four molecules. All three substituted acids (GA, HBA and PCA) yield high concentrations of H_2O_2 (Fig. 5d), since they are very reactive molecules that easily donate protons. Thus,

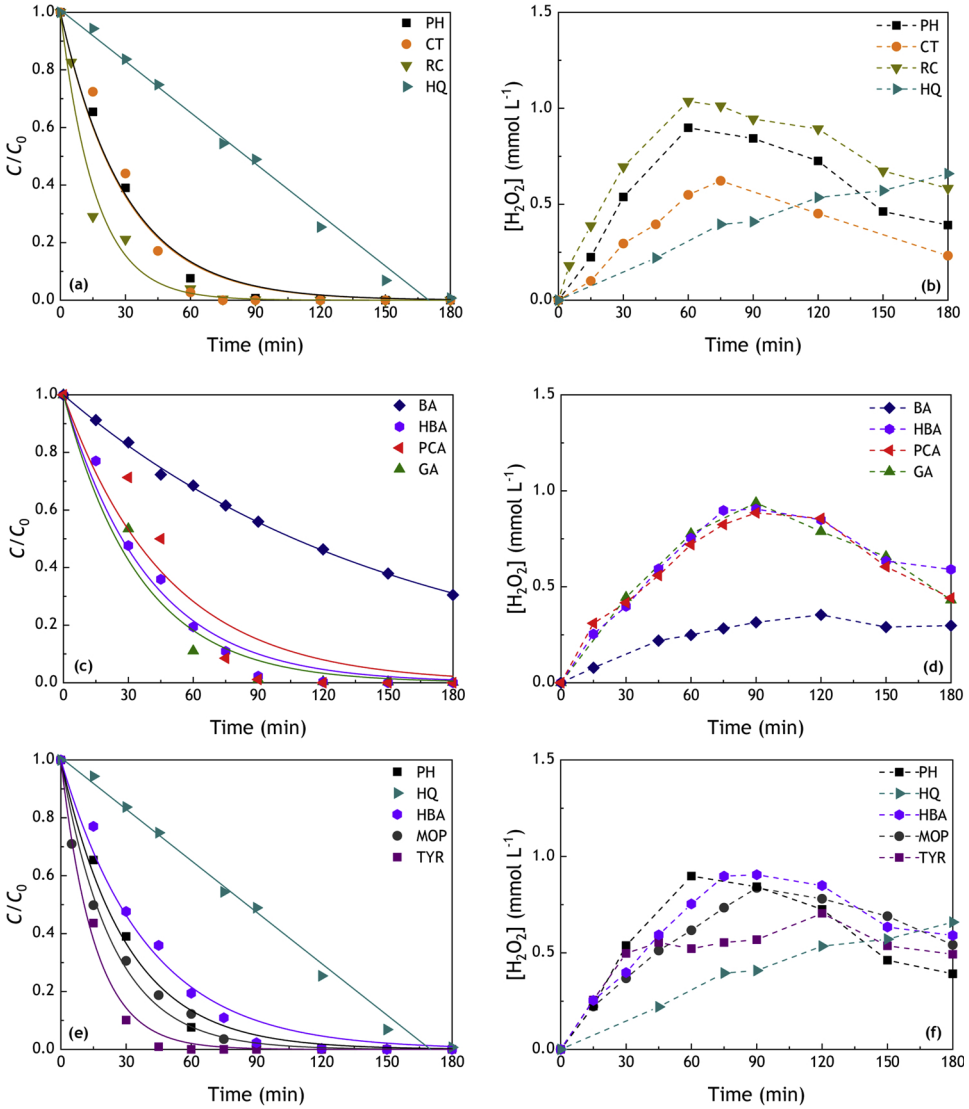

Fig. 5. (a, c, e) Normalized concentration of compounds and **(b, d, f)** H_2O_2 production during photocatalytic experiments to study the influence of substituent **(a, b)** position, **(c, d)** order and **(e, f)** nature.

it seems that more reactive compounds lead to higher H_2O_2 formation. In this case, GA, HBA and PCA showed maximum H_2O_2 amounts at 90 min (correspondingly, 0.047, 0.045 and 0.044 mmol of H_2O_2). The production of H_2O_2 in the presence of BA is slower, reaching 0.018 mmol of H_2O_2 at 120 min.

Different *para* substituted aromatic compounds were also studied: 4-methoxyphenol (MOP) has a methoxy group ($-OCH_3$), and tyrosol (TYR) has a hydroxyethyl group ($-CH_2CH_2OH$), both in the *para* position (Fig. 5e-f). TYR is more easily degraded than MOP and PH due to the presence of the −OH (*ortho* directing) and $-CH_2CH_2OH$ (*meta* directing) groups, allowing for a greater reactivity with two carbon atoms with more prone tendency to be attacked [40]. MOP holds a very strong (−OH) and a strong ($-OCH_3$) activating groups, resulting in a higher reactivity of the ring. Moreover, PH, HQ and BA are increasingly less reactive due to their own *para* substituents (−H, −OH and −COOH, respectively), as previously explained. Overall, it can be observed for all aromatic compounds studied that a faster degradation leads to higher H_2O_2 formation.

As previously explained, some compounds tend to be more easily attacked than others, as demonstrated by the k_{app} values listed in Table 1. Moreover, the TOC removals were above 70% in many cases, except for the more recalcitrant compounds, namely BA, MOP and TYR. The main contributors to the remaining TOC content are aliphatic acids, which are the final oxidation products detected at the end of the reaction. The low pH found (< 4) at the end of the reactions is in agreement with this hypothesis.

The rates of H_2O_2 production range from 625 (BA) to 3103 (RC) μmol $g_{cat}^{-1}\,h^{-1}$ (Table 1), which are significantly higher than in other metal-free photocatalytic processes [16–20,28,32,41–48]. The highest H_2O_2 production rate found in literature (3300 μmol $g_{cat}^{-1}h^{-1}$) was previously reported by Svoboda et al. [28], using 1.0 g L^{-1} of carbon nitride nanosheets produced from melamine, a 20 mg L^{-1} phenol solution under visible-LED irradiation (λ_{max} = 416 nm). In another work, Kofuji et al. [46] reported 550 μmol of H_2O_2 formation after 6 h of irradiation (and 150 μmol of H_2O_2 in 60 min), using 1.7 g L^{-1} of an hybrid catalyst of an imide-doped carbon nitride combined with reduced graphene oxide and boron nitride, a propan-2-ol/water (9:1 v/v) matrix and a Xe lamp (λ > 420 nm). For comparison purposes, one additional experiment was performed using 0.5 g L^{-1} of the gCN-T material studied in the present work and the same ratio of propan-2-ol in water, a H_2O_2 concentration of 480 μmol being obtained in 60 min. Typically, H_2O_2 evolution studies employ sacrificial agents (e.g., propan-2-ol, ethanol or butan-1-ol [16]), whereas the formation of H_2O_2 was accomplished in the present work with the simultaneous degradation of different pollutants acting as proton donors.

Finally, the possible influence of the pK_a of the studied compounds was also investigated. The selected compounds have pK_a values that range from ~4 (BA, HBA, PCA and GA) to ~10 (PH, CT, RC, HQ, MOP and TYR). The degradation and mineralization rates of these aromatic compounds were analysed and compared in terms of pK_a values. However, no correlations between pK_a and the photocatalytic results were found, these observations being in line with the amphoteric properties of gCN-T (Fig. 2). Thus, the nature, order and position of substituent groups on the aromatic ring seem to be the main responsible for the different efficiencies in the degradation and mineralization of the pollutants. Moreover, the pK_a does not affect the H_2O_2 production, which is mainly influenced by the DO content and the presence of more −OH groups in the aromatic ring.

3.6. Photocatalytic degradation and mineralization of a mixture of aromatic compounds

Considering the efficiency of gCN-T for the degradation of the different aromatic compounds, the photocatalytic treatment of a mixture containing ten compounds was performed. During this study, two mixtures were prepared: Mix A where the concentration of each compound was set at 0.640 mmol L^{-1}, and Mix B where a 20-fold dilution was employed (0.032 mmol L^{-1}). Results revealed that in the absence of catalyst both mixtures are relatively stable.

Regarding Mix A (Fig. 6a), it can be noticed that the photocatalytic

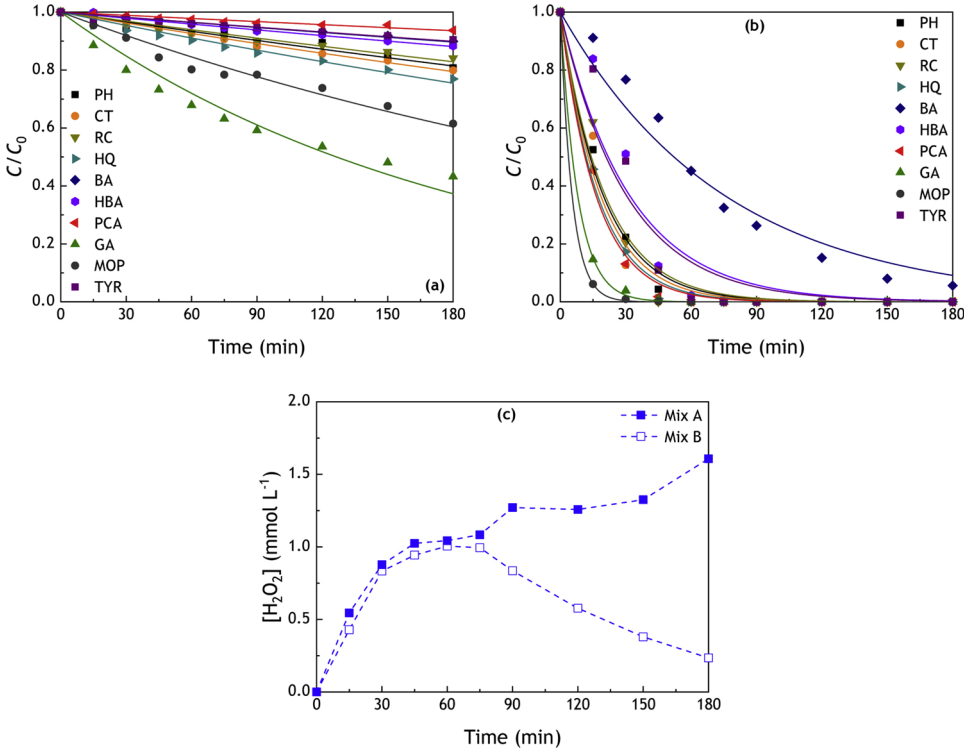

Fig. 6. Normalized concentration of the selected aromatic compounds in mixtures with **(a)** 0.640 mmol L^{-1} (Mix A) or **(b)** 0.032 mmol L^{-1} (Mix B) of each compound and **(c)** H_2O_2 production in each mixture.

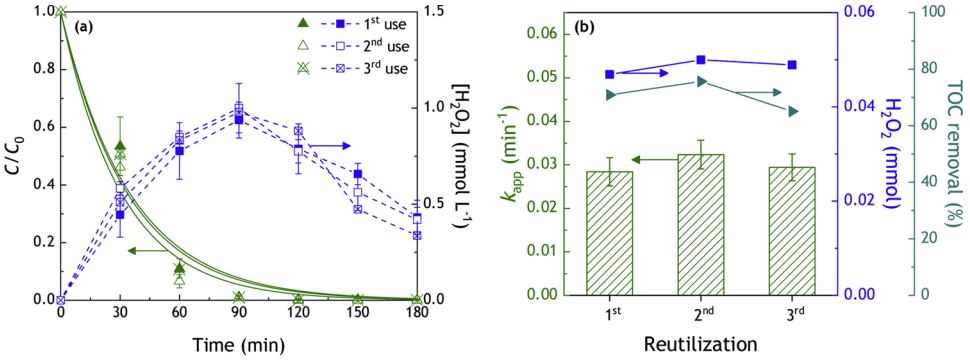

Fig. 7. (a) Gallic acid normalized concentration (C/C_0, C_0 = 0.640 mmol L^{-1}) and H_2O_2 production as a function of time and **(b)** apparent first-order reaction rate constant (k_{app}) with standard error from parameter fitting, H_2O_2 highest evolved amount -■- and TOC removal -►- after 180 min for each trial.

removal depends on the organic compound employed, GA being the easiest degraded (57% after 180 min), followed by MOP (38%). The remaining organics compounds show similar removals between 10 and 23%. No TOC removal was achieved at the end of the reaction. Analysing the results obtained with Mix B (Fig. 6b), nearly all compounds were completely removed in less than 180 min of irradiation, while 69.7% TOC removal was achieved, indicating that in this case organic compounds are oxidized to carbon dioxide and water.

Simultaneously, H_2O_2 was generated with both tested mixtures (Fig. 6c). Mix A yielded a maximum amount of 0.036 mmol at 180 min, which is expected yet to increase until the removal of all aromatics. Using Mix B, a highest H_2O_2 amount (0.023 mmol) was obtained at 60 min, when most compounds had already been completely removed. The reason behind the smaller yield obtained with Mix B is related to the lower initial concentration, as less initial substrate means the stoichiometry of H_2O_2 generation is disfavoured with fewer protons to form H_2O_2. However, it is observed that the H_2O_2 generation curve is quite similar for both mixtures until ca. 60 min. The initial concentration does not interfere with the rate of H_2O_2 production but with the extent of this reaction, i.e. the H_2O_2 concentration decreases in Mix B after 60 min, whereas the concentration continuously increases in Mix A. As discussed, a faster removal of aromatics was achieved in Mix B, consequently hindering further H_2O_2 evolution.

As explained in Section 3.5, each compound has a different reactivity towards oxidation. In this way, the observed removals and mineralization rates were somewhat expected. Moreover, some of the degradation rates obtained in the mixtures varied from those results where each compound was tested separately, possibly due to interference from the presence of the other aromatic compounds in the mixtures.

3.7. Catalyst reutilization tests

Since gallic acid (GA) generated one of the highest amounts of H_2O_2 (0.047 mmol in 90 min), and is the compound faster degraded in Mix A, it was selected to perform catalyst reutilization tests. The reusability of gCNT was demonstrated by performing consecutive photocatalytic runs using aqueous solutions of GA. In all runs, GA was rapidly degraded and completely removed after 90 min, when the maximum concentration of H_2O_2 was detected (Fig. 7a). The determined k_{app} values were also very similar in consecutive runs, ranging from 0.028 to 0.032 min^{-1}. Likewise, the mineralization rates were unchanged, TOC removals between 65 and 76% being obtained (Fig. 7b), as well as the pH (ca. 3.3 in 180 min). The H_2O_2 production was also similar, nearly overlapped evolution curves (Fig. 7a) and maximum values of 0.047, 0.050 and 0.049 mmol (Fig. 7b) being obtained for the 1st, 2nd and 3rd runs, respectively. All studied parameters, i.e. degradation rate, H_2O_2 production and TOC removal, remained constant throughout the experiments inferring that this material can be reused at least three times without losing its photocatalytic activity.

4. Conclusions

The studied metal-free carbon nitride material is highly active in the photocatalytic degradation of the tested aromatic compounds under visible light. The simultaneous in situ generation of H_2O_2 is ascribed to the photoactivation of the metal-free material in the presence of oxygen and at least one organic pollutant. Generally, larger amounts of H_2O_2 are obtained for the most reactive molecules. Moreover, the amphoteric properties of the material seem to play a key role in the degradation of these compounds, since the position, nature and order of the aromatic ring substituents affect the degradation regardless of the acidic/alkaline properties of each compound. Additionally, according to the reutilization tests, this material can be reused without showing any loss of photocatalytic activity.

Acknowledgments

This work was financially supported by project NORTE-01-0145-FEDER-031049 (InSpeCt) funded by FEDER funds through NORTE 2020 - Programa Operacional Regional do NORTE and by national funds (PIDDAC) through FCT/MCTES. We would also like to thank the scientific collaboration under project “AIProcMat@N2020 - Advanced Industrial Processes and Materials for a Sustainable Northern Region of Portugal 2020” (NORTE-01-0145-FEDER-000006, NORTE 2020, Portugal 2020 Partnership Agreement, through FEDER), project “Associate Laboratory LSRE-LCM” (UID/EQU/50020/2019 - FCT/MCTES - PIDDAC) and project “POCI-01-0145-FEDER-006984 – Associate Laboratory LSRE-LCM” (FEDER through COMPETE2020 - POCI and FCT). C.G.S. acknowledges the FCT Investigator Programme (IF/00514/2014) with financing from the European Social Fund (ESF) and the Human Potential Operational Programme.

Appendix A. Supplementary data

Supplementary material related to this article can be found, in the online version, at doi:https://doi.org/10.1016/j.apcatb.2019.03.040.

References

[1] L. Jiang, X. Yuan, G. Zeng, Z. Wu, J. Liang, X. Chen, L. Leng, H. Wang, H. Wang, Metal-free efficient photocatalyst for stable visible-light photocatalytic degradation of refractory pollutant, Appl. Catal. B-Environ. 221 (2018) 715–725.
[2] A. Kumar, A. Kumar, G. Sharma, M. Naushad, R.C. Veses, A.A. Ghfar, F.J. Stadler, M.R. Khan, Solar-driven photodegradation of 17-β-estradiol and ciprofloxacin from

waste water and CO_2 conversion using sustainable coal-char/polymeric-g-C_3N_4/RGO metal-free nano-hybrids, New J. Chem. 41 (2017) 10208–10224.
[3] Q. Wu, Y. He, H. Zhang, Z. Feng, Y. Wu, T. Wu, Photocatalytic selective oxidation of biomass-derived 5-hydroxymethylfurfural to 2,5-diformylfuran on metal-free g-C_3N_4 under visible light irradiation, Mol. Catal. 436 (2017) 10–18.
[4] C. Zhou, C. Lai, D. Huang, G. Zeng, C. Zhang, M. Cheng, L. Hu, J. Wan, W. Xiong, M. Wen, X. Wen, L. Qin, Highly porous carbon nitride by supramolecular pre-assembly of monomers for photocatalytic removal of sulfamethazine under visible light driven, Appl. Catal. B-Environ. 220 (2018) 202–210.
[5] W.-J. Ong, L.-L. Tan, Y.H. Ng, S.-T. Yong, S.-P. Chai, Graphitic carbon nitride (g-C_3N_4)-based photocatalysts for artificial photosynthesis and environmental remediation: are we a step closer to achieving sustainability? Chem. Rev. 116 (2016) 7159–7329.
[6] X. Li, J. Yu, M. Jaroniec, Hierarchical photocatalysts, Chem. Soc. Rev. 45 (2016) 2603–2636.
[7] H. Sun, G. Zhou, Y. Wang, A. Suvorova, S. Wang, A new metal-free carbon hybrid for enhanced photocatalysis, ACS Appl. Mater. Interfaces 6 (2014) 16745–16754.
[8] N.F.F. Moreira, M.J. Sampaio, A.R. Ribeiro, C.G. Silva, J.L. Faria, A.M.T. Silva, Metal-free g-C_3N_4 photocatalysis of organic micropollutants in urban wastewater under visible light, Appl. Catal. B-Environ. 248 (2019) 184–192.
[9] H. Li, Z. Bian, J. Zhu, Y. Huo, H. Li, Y. Lu, Mesoporous Au/TiO_2 nanocomposites with enhanced photocatalytic activity, J. Am. Chem. Soc. 129 (2007) 4538–4539.
[10] J.H. Pan, X. Zhang, A.J. Du, D.D. Sun, J.O. Leckie, Self-etching reconstruction of hierarchically mesoporous F-TiO_2 hollow microspherical photocatalyst for concurrent membrane water purifications, J. Am. Chem. Soc. 130 (2008) 11256–11257.
[11] S. Kumar, A. Kumar, A. Bahuguna, V. Sharma, V. Krishnan, Two-dimensional carbon-based nanocomposites for photocatalytic energy generation and environmental remediation applications, Beilstein J. Nanotechnol. 8 (2017) 1571–1600.
[12] G. Mamba, A.K. Mishra, Graphitic carbon nitride (g-C_3N_4) nanocomposites: a new and exciting generation of visible light driven photocatalysts for environmental pollution remediation, Appl. Catal. B-Environ. 198 (2016) 347–377.
[13] N. Barbero, D. Vione, Why dyes should not Be used to test the photocatalytic activity of semiconductor oxides, Environ. Sci. Technol. 50 (2016) 2130–2131.
[14] H. Wang, Y. Su, H. Zhao, H. Yu, S. Chen, Y. Zhang, X. Quan, Photocatalytic oxidation of aqueous ammonia using atomic single layer graphitic-C_3N_4, Environ. Sci. Technol. 48 (2014) 11984–11990.
[15] Y. Cui, J. Huang, X. Fu, X. Wang, Metal-free photocatalytic degradation of 4-chlorophenol in water by mesoporous carbon nitride semiconductors, Catal. Sci. Technol. 2 (2012) 1396–1402.
[16] Y. Shiraishi, S. Kanazawa, Y. Sugano, D. Tsukamoto, H. Sakamoto, S. Ichikawa, T. Hirai, Highly selective production of hydrogen peroxide on graphitic carbon nitride (g-C_3N_4) photocatalyst activated by visible light, ACS Catal. 4 (2014) 774–780.
[17] Y. Shiraishi, Y. Kofuji, H. Sakamoto, S. Tanaka, S. Ichikawa, T. Hirai, Effects of surface defects on photocatalytic H_2O_2 production by mesoporous graphitic carbon nitride under visible light irradiation, ACS Catal. 5 (2015) 3058–3066.
[18] H.-i. Kim, Y. Choi, S. Hu, W. Choi, J.-H. Kim, Photocatalytic hydrogen peroxide production by anthraquinone-augmented polymeric carbon nitride, Appl. Catal. B-Environ. 229 (2018) 121–129.
[19] S. Zhao, T. Guo, X. Li, T. Xu, B. Yang, X. Zhao, Carbon nanotubes covalent combined with graphitic carbon nitride for photocatalytic hydrogen peroxide production under visible light, Appl. Catal. B-Environ. 224 (2018) 725–732.
[20] H. Zhang, L.-H. Guo, L. Zhao, B. Wan, Y. Yang, Switching oxygen reduction pathway by exfoliating graphitic carbon nitride for enhanced photocatalytic phenol degradation, J. Phys. Chem. Lett. 6 (2015) 958–963.
[21] C. Liu, Y. Zhang, F. Dong, X. Du, H. Huang, Easily and synchronously ameliorating charge separation and band energy level in porous g-C_3N_4 for boosting photo-oxidation and photoreduction ability, J. Phys. Chem. C 120 (2016) 10381–10389.
[22] Y. Cui, Z. Ding, P. Liu, M. Antonietti, X. Fu, X. Wang, Metal-free activation of H_2O_2 by g-C_3N_4 under visible light irradiation for the degradation of organic pollutants, Phys. Chem. Chem. Phys. 14 (2012) 1455–1462.
[23] M.J. Lima, A.M.T. Silva, C.G. Silva, J.L. Faria, Graphitic carbon nitride modified by thermal, chemical and mechanical processes as metal-free photocatalyst for the selective synthesis of benzaldehyde from benzyl alcohol, J. Catal. 353 (2017) 44–53.
[24] G. Eisenberg, Colorimetric determination of hydrogen peroxide, Ind. Eng. Chem. Anal. Ed. 15 (1943) 327–328.
[25] P. Xia, B. Zhu, J. Yu, S. Cao, M. Jaroniec, Ultra-thin nanosheet assemblies of graphitic carbon nitride for enhanced photocatalytic CO_2 reduction, J. Mater. Chem. A Mater. Energy Sustain. 5 (2017) 3230–3238.
[26] B. Zhu, P. Xia, W. Ho, J. Yu, Isoelectric point and adsorption activity of porous g-C_3N_4, Appl. Surf. Sci. 344 (2015) 188–195.
[27] M. Fronczak, M. Krajewska, K. Demby, M. Bystrzejewski, Extraordinary adsorption of methyl blue onto sodium-doped graphitic carbon nitride, J. Phys. Chem. C 121 (2017) 15756–15766.
[28] L. Svoboda, P. Praus, M.J. Lima, M.J. Sampaio, D. Matýsek, M. Ritz, R. Dvorský, J.L. Faria, C.G. Silva, Graphitic carbon nitride nanosheets as highly efficient photocatalysts for phenol degradation under high-power visible LED irradiation, Mater. Res. Bull. 100 (2018) 322–332.
[29] J. Li, Y. Liu, H. Li, C. Chen, Fabrication of g-C_3N_4/TiO_2 composite photocatalyst with extended absorption wavelength range and enhanced photocatalytic performance, J. Photochem. Photobiol. A: Chem. 317 (2016) 151–160.
[30] J.-M. Herrmann, Titania-based true heterogeneous photocatalysis, Environ. Sci. Pollut. Res. 19 (2012) 3655–3665.
[31] M.J. Sampaio, C.G. Silva, A.M.T. Silva, J.L. Faria, Kinetic modelling for the photocatalytic degradation of phenol by using TiO_2-coated glass raschig rings under simulated solar light, J. Chem. Technol. Biotechnol. 91 (2016) 346–352.
[32] Y. Kofuji, S. Ohkita, Y. Shiraishi, H. Sakamoto, S. Tanaka, S. Ichikawa, T. Hirai, Graphitic carbon nitride doped with biphenyl diimide: efficient photocatalyst for hydrogen peroxide production from water and molecular oxygen by sunlight, ACS Catal. 6 (2016) 7021–7029.
[33] P.M. Wood, The potential diagram for oxygen at pH 7, Biochem. J. 253 (1988) 287–289.
[34] M.J. Sampaio, R.R. Bacsa, A. Benyounes, R. Axet, P. Serp, C.G. Silva, A.M.T. Silva, J.L. Faria, Synergistic effect between carbon nanomaterials and ZnO for photocatalytic water decontamination, J. Catal. 331 (2015) 172–180.
[35] G.A. Somorjai, Active sites in heterogeneous catalysis, in: D.D. Eley, H. Pines, P.B. Weisz (Eds.), Advances in Catalysis, Academic Press, 1977, pp. 1–68.
[36] W. Ding, S. Liu, Z. He, One-step synthesis of graphitic carbon nitride nanosheets for efficient catalysis of phenol removal under visible light, Chin. J. Catal. 38 (2017) 1711–1718.
[37] M.J. Sampaio, C.G. Silva, A.M.T. Silva, V.J.P. Vilar, R.A.R. Boaventura, J.L. Faria, Photocatalytic activity of TiO_2-coated glass raschig rings on the degradation of phenolic derivatives under simulated solar light irradiation, Chem. Eng. J. 224 (2013) 32–38.
[38] A.M.T. Silva, E. Nouli, N.P. Xekoukoulotakis, D. Mantzavinos, Effect of key operating parameters on phenols degradation during H_2O_2-assisted TiO_2 photocatalytic treatment of simulated and actual olive mill wastewaters, Appl. Catal. B-Environ. 73 (2007) 11–22.
[39] A.M.T. Silva, E. Nouli, Â.C. Carmo-Apolinário, N.P. Xekoukoulotakis, D. Mantzavinos, Sonophotocatalytic/H_2O_2 degradation of phenolic compounds in agro-industrial effluents, Catal. Today 124 (2007) 232–239.
[40] T.W.G. Solomons, C. Fryhle, Organic Chemistry, 10th ed., John Wiley & Sons Inc, New York, 2009.
[41] Y. Shiraishi, S. Kanazawa, Y. Kofuji, H. Sakamoto, S. Ichikawa, S. Tanaka, T. Hirai, Sunlight-driven hydrogen peroxide production from water and molecular oxygen by metal-free photocatalysts, Angew. Chem. Int. Ed. English 53 (2014) 13454–13459.
[42] Y. Kofuji, Y. Isobe, Y. Shiraishi, H. Sakamoto, S. Tanaka, S. Ichikawa, T. Hirai, Carbon nitride-aromatic diimide-graphene nanohybrids: metal-free photocatalysts for solar-to-Hydrogen peroxide energy conversion with 0.2% efficiency, J. Am. Chem. Soc. 138 (2016) 10019–10025.
[43] S. Li, G. Dong, R. Hailili, L. Yang, Y. Li, F. Wang, Y. Zeng, C. Wang, Effective photocatalytic H2O2 production under visible light irradiation at g-C_3N_4 modulated by carbon vacancies, Appl. Catal. B-Environ. 190 (2016) 26–35.
[44] Y. Kofuji, S. Ohkita, Y. Shiraishi, H. Sakamoto, S. Ichikawa, S. Tanaka, T. Hirai, Mellitic triimide-doped carbon nitride as sunlight-driven photocatalysts for hydrogen peroxide production, ACS Sustain. Chem. Eng. 5 (2017) 6478–6485.
[45] L. Yang, G. Dong, D.L. Jacobs, Y. Wang, L. Zang, C. Wang, Two-channel photocatalytic production of H_2O_2 over g-C_3N_4 nanosheets modified with perylene imides, J. Catal. 352 (2017) 274–281.
[46] Y. Kofuji, Y. Isobe, Y. Shiraishi, H. Sakamoto, S. Ichikawa, S. Tanaka, T. Hirai, Hydrogen peroxide production on a carbon nitride–Boron nitride-reduced graphene oxide hybrid photocatalyst under visible light, ChemCatChem 10 (2018) 2070–2077.
[47] R. Wang, X. Zhang, F. Li, D. Cao, M. Pu, D. Han, J. Yang, X. Xiang, Energy-level dependent H_2O_2 production on metal-free, carbon-content tunable carbon nitride photocatalysts, J Energy Chem 27 (2018) 343–350.
[48] Z. Zhu, H. Pan, M. Murugananthan, J. Gong, Y. Zhang, Visible light-driven photocatalytically active g-C_3N_4 material for enhanced generation of H_2O_2, Appl. Catal. B-Environ. 232 (2018) 19–25.